Theoretical Ecology (2025) 18:13
https://doi.org/10.1007/s12080-025-00607-w

RESEARCH

Shared preferences along stress gradients: how a growth-tolerance trade-off drives unimodal diversity and trait lumping

Torben Schucht[1] · **Bernd Blasius**[1,2]

Received: 2 December 2024 / Accepted: 10 March 2025

Abstract

Environmental gradients are pervasive across ecosystems and play a fundamental role in structuring species distributions and community dynamics. While ecological theory mainly focuses on species with distinct preferences for specific niches along the gradient, many natural communities follow an alternative pattern of shared preferences. In such systems, all species prefer the same optimal conditions but differ in their tolerance to harsher environments, according to a growth-tolerance trade-off. Here, we develop a trait-based metacommunity model, based on integrodifference equations, to investigate the development of community structure along a one-dimensional stress gradient with shared preferences. We demonstrate how species interactions, driven by competition, dispersal, and a growth-tolerance trade-off, lead to the emergence of patterns such as unimodal diversity distributions and trait lumping. Our model provides a conceptual framework for exploring the processes that shape metacommunities across spatial gradients characterized by shared preferences, offering new insights into this underrepresented class of ecological systems.

Keywords Shared preferences · Stress gradients · Unimodal diversity · Trait lumping · Growth-tolerance trade-off · Integrodifference model

Introduction

Life in nature unfolds along gradients, shaping ecological communities across diverse landscapes. One of the most prominent and well-documented patterns in ecology is the spatial zonation of species along environmental gradients. This turnover of species is observed across a wide range of taxa and environmental factors, including temperature, elevation, latitude, light, water depth, salinity, and nutrient availability (Whittaker 1967a, b; Wellborn et al. 1996; Körner 2007; Telesh et al. 2013). Environmental gradients provide a powerful lens to study species dynamics and are widely used to predict shifts in species distributions in response to environmental change. However, the relationship between spatial gradients and temporal changes is complex, as species abundances are shaped not only by abiotic factors but also by biotic interactions such as dispersal, competition, and facilitation. Predictions based solely on spatial observations may therefore be misleading without a deeper understanding of the underlying ecological mechanisms. This highlights the need to unravel the mechanisms that drive species performance and interactions along environmental gradients.

The classic model of competition along environmental gradients centers on the concept of distinct preferences (Rosenzweig 1991; Anderson et al. 2022). In this model, each species occupies an optimal niche segment along the gradient, distinct from the others, where it has its highest performance—known as its fundamental niche (Hutchinson 1957; Colwell & Fuentes 1975). As environmental conditions deviate from this optimal point, species performance declines (Fig. 1a). The concept of distinct preferences was formalized in the seminal models by MacArthur and Levins (1967) and MacArthur et al. (1972), profoundly shaping ecological thinking about competition along environmental gradients. These models show that competition and niche overlap reduce the realized niche (the actual space a species occupies), but

✉ Bernd Blasius
bernd.blasius@uni-oldenburg.de

[1] Institute for Chemistry and Biology of the Marine Environment (ICBM), University of Oldenburg, Oldenburg, Germany

[2] Helmholtz Institute for Functional Marine Biodiversity (HIFMB), Oldenburg, Germany

Published online: 22 March 2025

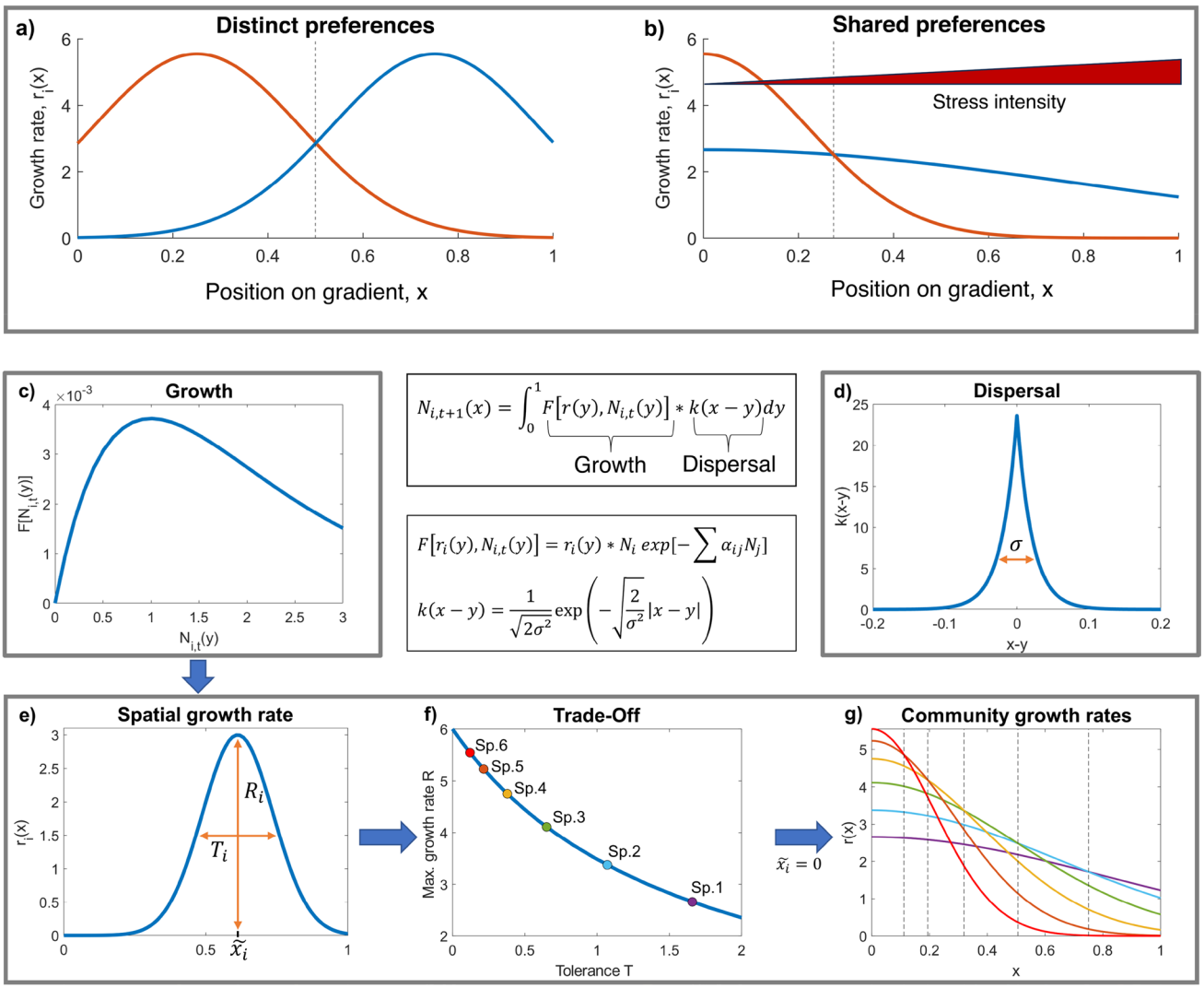

Fig. 1 Conceptual framework of the gradient model and growth-tolerance trade-off. (Top) Illustration of species-specific growth rates $r_i(x)$ along two types of spatial gradients. **a** Distinct preferences: species achieve optimal growth at different abiotic conditions x. **b** Shared preferences along a stress gradient: both species obtain highest growth at the benign end ($x = 0$) where stress is minimal (stress level indicated by the red arrow). Coexistence is driven by a growth-tolerance trade-off. The growth-specialist (red) exhibits a high relative growth rate but lower tolerance, dominating the low-stress region (left side of the gradient). In contrast, the tolerant species (blue) has lower growth but higher tolerance, allowing it to persist under higher stress (right side of the gradient). (Middle) Model overview. The population density $N_{i,t+1}$ of species i at time step $t + 1$ is computed by combining population growth with spatial dispersal. **c** Growth follows a Ricker function $F[N_i] = r_i(y)N_i \exp\left[-\sum_j \alpha_{ij}N_j\right]$ with growth rate $r_i(y)$ and competition coefficients α_{ij}. **d** Dispersal is modelled as a Laplace distribution $k(x - y)$ of width σ. (Bottom) Growth-tolerance trade-off. **e** Growth rates $r_i(x)$ vary along the gradient x as a Gaussian function with standard deviation T_i (species tolerance) and maximal growth R_i at location $\tilde{x}_i$. To model a stress gradient, we set $\tilde{x}_i = 0$, causing growth rates to be maximized at the benign end of the gradient. **f** Tolerance T_i and maximum growth rate R_i are derived from a trade-off curve, shown for a community of six species (circles). **g** Resulting growth profiles $r_i(x)$. Growth-specialists (e.g., Sp. 6, red) display sharp growth peaks but perform poorly under stress, whereas more tolerant species (e.g., Sp. 1, purple) show lower peak growth but maintain moderate growth across higher stress levels. Dashed lines mark transitions between the dominant species across the gradient

species tend to concentrate around their region of peak performance, resulting in spatial segregation with partly overlapping but distinct unimodal distributions (Whittaker 1967a, b).

While this model applies to many gradients and remains the foundation for most ecological studies, many communities follow an alternative form of niche organization characterized by shared preferences (Rosenzweig 1991; Wisheu 1998; McGill et al. 2006). In this scenario, all species share a common preference for the same optimal region along the gradient, but they differ in their tolerance to less favorable conditions. The ability

to dominate the most productive sites comes at the cost of being less capable to survive in marginal or harsh environments, resulting in a growth-tolerance trade-off, where intolerant, growth-specialized species dominate the preferred ranges of the gradient, while more tolerant, subordinate species persist in suboptimal conditions. In these systems, the fundamental niches of dominant species are nested within the broader niches of more tolerant species—the inclusive fundamental niche (Colwell & Fuentes 1975)—leading to a competitive hierarchy that governs species distribution along the gradient (Fig. 1b).

Numerous case studies have demonstrated the widespread occurrence of growth-tolerance trade-offs, particularly along stress gradients where survival becomes increasingly difficult as conditions grow harsher (McGill et al. 2006). Stress gradients are found globally, driven by factors such as elevation in mountains, light availability in aquatic environments, and salinity or physical stress in salt marshes (Pennings & Bertness 2001). For instance, studies on the range limits of North American trees show that many boreal species achieve their optimal growth in temperate climates beyond their southern range, while their realized boundaries are constrained by a trade-off between allocating resources to either maximal height growth or freezing tolerance (Loehle 1998). Similar patterns have been observed across different taxonomic groups, including plants along salinity gradients (Snow & Vince 1984; Crain et al. 2004), herbaceous plants along hydrological gradients (Tittes et al. 2019), insects along salinity gradients (Arribas et al. 2019), and mosses along nutrient gradients (Jaszczuk et al. 2023)—in each case showing that species only observed at the hostile end of the gradient were performing far better at the benign end in the absence of competitors.

Despite the widespread evidence of shared preferences, most theoretical investigations have focused on the distinct preference model. Although it has long been speculated that shared preferences could yield regular zonation patterns (Colwell & Fuentes 1975; Rosenzweig 1991), these ideas have rarely been explored in mathematical models. Notable exceptions include the tolerance-fecundity model proposed by Muller-Landau (2010) and subsequent studies by D'Andrea et al. (2013) and D'Andrea and O'Dwyer (2021), which examine the trade-off between seed survivability and seed number at different stress levels. One key aim of this paper is to develop a framework for investigating community processes along environmental gradients where species share similar preferences. By doing so, we aim not only to improve our understanding of community processes acting in such systems but also to explain two emergent patterns: (i) unimodal diversity distributions and (ii) clustering of species traits, known as trait lumping.

Unimodal diversity gradients

In classic continuum theory (Gauch & Whittaker 1972), species distributions are expected to follow a linear, evenly spaced pattern, akin to a regular chain (Whittaker 1967a, b). In contrast, Grime (1973) proposed that biodiversity will be highest at intermediate levels of productivity. This pattern frequently arises along stress gradients, where species richness peaks at intermediate levels of stress. Grime's theory suggests that highly productive environments foster competitive exclusion, reducing local diversity. At intermediate stress, the performance of dominant species declines, allowing less competitive species to survive and coexist, while at extreme levels of stress, many species struggle to survive, causing a drop in diversity. This results in a characteristic unimodal or hump-shaped diversity pattern along the stress gradient. As was demonstrated in a meta-analysis on species diversity patterns (Mittelbach et al. 2001), hump-shaped diversity patterns were observed in most empirical studies, and they occur across various ecosystems, including the marine intertidal zone (Sousa 1979; Zwerschke et al. 2013), elevation gradients (Grytnes & Vetaas 2002; Guo et al. 2013; Mumladze et al. 2023), and natural salt marshes (Suchrow & Jensen 2010; Kim & Ohr 2020; Bauer et al. 2021). Despite this prevalence of hump-shaped diversity patterns, not much is known about its underlying mechanisms.

Trait lumping

A long-standing theory in ecology posits that the intensity of interspecific competition increases as species become more similar, suggesting that coexisting species should display significant trait differences (Leibold 1998; Anten & Hirose 1999; Schamp et al. 2008; Letten et al. 2017). However, alternative theories propose that competition in environmental gradients may cause species to self-organize into clusters with similar trait values, a phenomenon known as "trait lumping" (Scheffer & van Nes 2006). This contradicts the intuitive assumption that gradual variation in environmental conditions should correspond to gradual shift in species traits. Trait lumping has been identified as a generic feature of competitive dynamics (D'Andrea et al. 2019), and pattern formation theory explains how these clusters emerge (Pigolotti et al. 2007; Delfau et al. 2016). Numerous studies have demonstrated that trait lumping is a robust phenomenon, occurring under fluctuating conditions (Sakavara et al. 2017) and in spatially extended systems (Doebeli and Dieckmann 2003; Leimar et al. 2008; Norberg et al. 2012; Mohammed et al. 2022). Nevertheless, it remains unclear whether trait lumping occurs along stress gradients and how it interacts with hump-shaped diversity patterns.

In this paper, we develop a conceptual model framework to study community patterns and diversity distributions along

a stress gradient with shared preferences. Our model adopts the metacommunity paradigm, describing a system of multiple communities that are connected by dispersal (Wilson 1992; Leibold et al. 2004, 2017). Following a recently proposed trait-based metacommunity framework that links local coexistence theory with spatial processes (Thompson et al. 2020), we define community dynamics by three fundamental processes: (i) density-independent species growth rates based on local abiotic conditions, (ii) density-dependent intra- and interspecific competition, and (iii) dispersal which influences population sizes based on the distance between communities. We model this on a one-dimensional spatially continuous gradient using integrodifference equations (Lutscher 2019) and introduce a trade-off between maximal growth rate and tolerance, reflecting shared preferences. This approach allows us to examine the mechanisms that determine biodiversity patterns and the relationship between fundamental and realized niches along stress gradients. By focusing on systems with shared preferences, we aim to clarify the role of growth-tolerance trade-offs in structuring these communities, shedding light on the temporal development of community structure and the formation of phenomena such as hump-shaped diversity patterns, trait lumping, and extinction cascades. This investigation will provide a deeper understanding into the processes governing biodiversity in systems characterized by shared preferences and offer new insights into this underrepresented class of ecological systems.

Materials and methods

Model description

Our model builds on the metacommunity framework recently introduced by Thompson et al. (2020) to simulate the population dynamics of S interacting species that grow, compete, and disperse along a stress gradient x (Fig. 1). The model operates in discrete time steps within a continuous spatial domain from $0 \leq x \leq 1$ and tracks the population densities $N_{i,t}(x)$ of a community of species i at position x and time t. This is done using an integrodifference equation (Lutscher 2019), which combines local growth and dispersal dynamics:

$$N_{i,t+1}(x) = \int_0^1 F\left[r(y), N_{i,t}(y)\right] k(x-y)dy \tag{1}$$

Population growth F (Fig. 1c) is modelled as a Ricker function (Ricker 1954):

$$F\left[r_i(y), N_i(y)\right] = r_i(y)N_i exp[-\sum \alpha_{ij}N_j] \tag{2}$$

It consists of a density-independent spatial growth rate, $r_i(y)$, (see below) and density-dependent species interactions determined by the competition coefficients α_{ij}, accounting for both interspecific ($i \neq j$) and intraspecific ($i = j$) effects. For simplicity, we assume neutral competition, setting $\alpha_{ij} = 1$ for all species.

After the local population growth is determined, the model incorporates the dispersal of propagules across space. Dispersal is represented by a dispersal kernel, $k(x-y)$, which describes the probability of an individual moving from position y to position x. Here, we use a symmetric Laplace kernel with standard deviation σ (Fig. 1d):

$$k(x-y) = \frac{1}{\sqrt{2\sigma^2}} exp\left(-\sqrt{\frac{2}{\sigma^2}}|x-y|\right) \tag{3}$$

The abiotic niche of a species is captured through its growth rate $r_i(x)$, which depends on the species' position along the gradient x. This rate is modelled as a Gaussian response curve:

$$r_i(x) = R_i exp\left(-\frac{|x-\hat{x}_i|^2}{2T_i}\right) \tag{4}$$

where R_i is the species' maximum growth rate and T_i represents its tolerance, indicating how rapidly growth is reduced by the mismatch between x and the position of optimal growth $\hat{x}_i$ (Fig. 1e). The shape of this response curve governs the range of abiotic conditions for which positive growth is possible, that is, where $r_i(x) > 1$.

While most gradient-based models assume different optimal growth positions for each species (Fig. 1a), we simulate a stress gradient with optimal growth position $\hat{x}_i = 0$ for all species, where growth peaks at the benign end and declines as stress increases towards the hostile end, $x = 1$ (Fig. 1b). To prevent species from becoming super competitors with both high maximum growth rates R_i and high tolerance T_i, we impose a trade-off between these parameters. Species with high tolerance T_i can sustain better growth under stressful conditions, which comes at the cost of lower maximal growth rate R_i. Each species is assigned a unique combination of R_i and T_i based on its trait value θ_i, which defines its position on the trade-off curve (Wickman et al. 2017) (Fig. 1f):

$$R_i = \frac{R_{max}}{1 + \exp[-(\beta + \theta_i)]} + 1 \tag{5}$$

$$T_i = \frac{T_{max}}{1 + \exp[-\beta + \theta_i]} \tag{6}$$

The parameters R_{max} and T_{max} define the upper limits of a species' potential growth rate and tolerance at the extreme ends of the trade-off curve. To ensure that each species maintains a maximal growth rate of $R_i \geq 1$, we

added a constant of 1 to the equation for R_i. This adjustment prevents the inclusion of species which would not be able to survive anywhere along the gradient, even in the absence of stress. The parameter β controls the curvature of the trade-off curve. For our simulations, we used a slightly convex trade-off curve with $\beta = -0.7$ (Fig. 1f).

Trait values for species within the community are distributed with equidistant spacing across the interval $\theta_i \in [0, \theta_{max}]$. This creates a distinct spatial growth curve $r_i(x)$ for each species (Figs. 1g and 7). The trait interval $[0, \theta_{max}]$ is calibrated so that the species with the highest tolerance achieves a growth rate slightly greater than one at the most hostile end of the gradient, $r_1(1) \geq 1$. This design ensures that at every point along the gradient, at least one species exhibits positive growth, effectively covering the entire gradient and preventing uninhabitable zones due to extreme stress levels. The resulting growth rate curves, illustrated in Fig. 1g, demonstrate how, due to the trade-off, each species dominates a specific region of the gradient (separated by vertical dashed lines in the figure). Within these regions, each species attains the highest growth rate compared to others, making it the best-adapted species in that specific zone of the gradient.

To quantify biodiversity in the simulated communities, we use the effective species richness based on the Shannon index $S_{Sh}[p] = \exp\left(-\sum_i p_i \ln(p_i)\right)$ with the relative species densities $p_i = N_i / \sum_i N_i$ (Jost 2006). Computing this index locally at each position along the gradient yields the local diversity $D_l(x) = S_{Sh}[p(x)]$, which is a spatial function of x. For numerical implementation, we divide the gradient into bins, each consisting of four cells, and compute the diversity in each bin. Additionally, we compute the average local diversity $D_{av} = \int S_{Sh}[p(x)]dx$ and the global diversity, defined as the Shannon index of the spatially averaged relative density $D_{glob} = S_{Sh}\left[\int p(x)dx\right]$ (Mohammed et al. 2022).

Numerical implementation and parameter values

The model is implemented and simulated in MATLAB. To enhance computational efficiency, the convolutions in the integrodifference Eq. (1) are computed using fast Fourier transforms, as described by Powell (2001). The spatial component incorporates closed boundary conditions, which are implemented using a technique outlined by Andersen (1991) and adapted for MATLAB by Lutscher (2019). For reproducibility and further research, the source code to reproduce the results and the figures is publicly available at the research repository Zenodo: https://doi.org/10.5281/zenodo.14163043.

We used a spatial resolution of $L = 1024$ cells. To save computation time, this value was lowered to $L = 512$ in the simulation with the larger community of 500 species, while it was increased to $L = 4096$ in the dispersal simulation, as this was essential to provide accurate results at low dispersal.

Species are considered extinct when their total density across the entire gradient, $\int_0^1 N_i(x)dx$, falls below a critical threshold. Once this extinction threshold is crossed, the density $N_i(x)$ for that species is set to 0, after which the species is permanently removed from the system and cannot recover from the extinction event.

As a simplification, all species are assigned the same dispersal range of $\sigma = 0.02$. This value proved to be an optimal balance, enabling species to effectively distribute themselves along the gradient, while minimizing the loss of propagules beyond the simulated domain (we later examine the effects of varying dispersal strengths in more detail). At the start of each multi-species simulation, species densities are uniformly initialized at 0.01 across all positions on the gradient, ensuring that no species has an advantage at the start and that initially, every species is present everywhere on the gradient. This choice of initial conditions, however, had no influence on the long-term outcome, as we did not observe any evidence of multi-stability in the simulations. The maximal duration of the simulations was set to 10^6. A complete list of all used model parameters is provided in Table 1.

Results

We begin by analyzing the build-up of spatial density profiles in small communities. For a single species starting from a small initial density (Fig. 2a–e), the population initially grows locally before expanding as a travelling wave across the domain. After about 100 time steps, intraspecific competition limits further growth, resulting in a stationary density profile where population density gradually declines towards the stressful end of the gradient, eventually dropping to zero once $r_i(x) < 1$ (note that due to source-sink effects caused by dispersal, the actual species range is slightly extending beyond this point). Additionally, a sharp decline in density occurs at the benign end ($x = 0$), extending over a distance roughly equal to the width σ of the dispersal kernel. This decline is caused by boundary effects as many propagules disperse over this boundary, reducing the population near the edge.

In multi-species communities, spatial organization follows the relative positions of species on the trade-off curve. Species with the highest intrinsic growth rates dominate the benign end of the gradient, while more tolerant species dominate at the stressful end. This is shown in Fig. 2f–j for the case of two species: a fast-growing species (red) and

Table 1 Variables and parameters used in the model

Symbol	Description	Value
β	Shape of trade-off curve (concave/convex)	-0.7
T_{max}	Max. value of tolerance, T	5
R_{max}	Max. value of maximum growth rate, R	5
α_{ij}	Competition coefficients (used for all species interactions)	1
L	Spatial resolution of gradient x	1024[a];512[b];4096[c]
S	Number of generated species	1[a];2[a];25[a, c];500[b]
θ_{max}	Maximum position on trade-off axis	3
$\widetilde{x}$	Position of optimal growth	0
N_{crit}	Extinction threshold (sum across whole space)	0.01
$N_{i,0}(x)$	Initial density	0.01
σ	Dispersal width	0.02[a,b];0.005 – 0.05[c]

[a]Simulations related to Figs. 2 and 3 with 1, 2, or 25 species

[b]Simulation related to Fig. 4 with 500 species

[c]Simulations related to Fig. 5 with different dispersal rates and 25 species

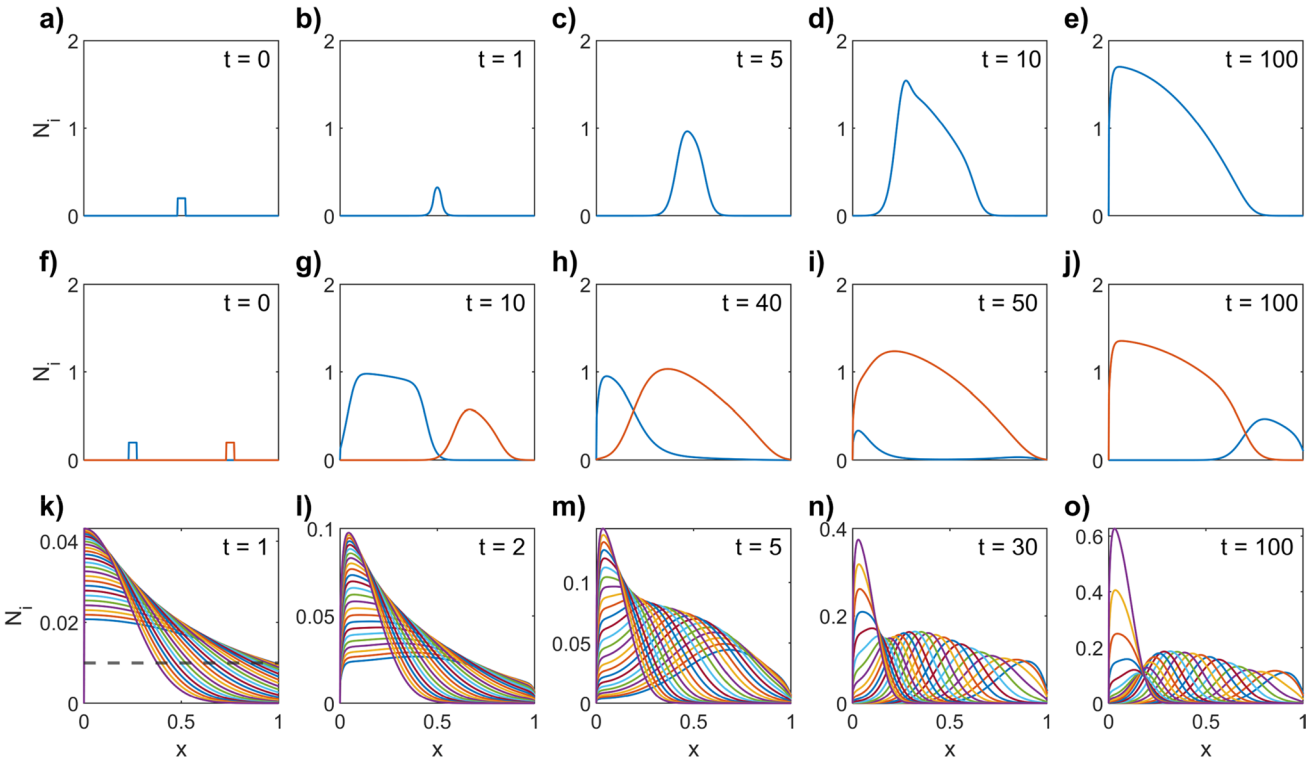

Fig. 2 Development of spatial profiles over the first 100 time steps. The figure presents the simulated spatial profiles $N_{i,t}(x)$ at five selected time points for three different community setups: **a–e** A single population with traits $T_i = 0.4$ and $R_i = 5.5$ is initially introduced with a small localized density, $N_{i,0} = 0.2$, in the center of the gradient around $x = 0.5$. The progression of the population distribution is shown as it spreads across the spatial gradient. **f–j** A two-species community (similar to Fig. 1b), consisting of a growth-specialist ($T_i = 0.8, R_i = 3.9$, red line), initially located around $x = 0.75$, and a stress-tolerant species ($T_i = 1.7, R_i = 2.7$, blue line), initially located around $x = 0.25$. The time series shows how these species interact and adjust their spatial distributions over the gradient during the simulation. **k–o** A community of 25 species, with trait values equally spaced on the trade-off curve (see Methods and Fig. 7). The species are initially distributed homogeneously along the gradient at low densities ($N_{i,0} = 0.01$). The panels show the progression of the spatial profiles, highlighting the spatial segregation and species distribution across the gradient at the early stages of the simulation. Note that the initial density of all species is depicted in k as a dashed black line

a more tolerant, slower-growing species (blue). Initially, each species starts from a small, localized population, with the tolerant species near the benign end and the growth-specialist near the stressful end of the gradient. Over time, both species grow in density and expand their ranges. However, the growth-specialist eventually invades and dominates the benign end, outcompeting the tolerant species, which is then confined to the stressful end of the gradient. This leads the tolerant species to form a unimodal density profile with a maximum near $x \approx 0.75$(blue curve in Fig. 2j), despite its intrinsic growth rate being located around $x = 0$. This example demonstrates that even with just two species, the system can undergo complex transitions, such as reversing the positions of spatial dominance during the approach to equilibrium.

This environmental sorting occurs rapidly even in larger communities. Figure 2k–o shows the short-term dynamics in a community of 25 species with trait values evenly distributed along the trade-off curve (see also Fig. 7) and starting from identical homogenous initial conditions of small density. Initially, all species grow in density, with higher growth rates at the benign end of the gradient, reflecting the shapes of their growth functions. However, as overall density increases, competition intensifies, causing each species to dominate in the region where it has a higher intrinsic growth rate than all others. As a consequence, species' density profiles become unimodal, localized in small regions, and sorted in space according to their positions on the trade-off curve. The highest density maxima occur at the benign end of the gradient, which suppresses growth in adjacent regions ($x \approx 0.25$), creating a characteristic density minimum in this area (Fig. 2o).

Beyond this initial sorting in space, the community undergoes further reorganization over longer time scales, leading to noticeable changes in the community structure (Figs. 3 and 8). Thereby, the density curves of many species shift towards the middle of the gradient. Additionally, several species near the ends of the gradient become extinct, further accelerating this shift. Despite these changes and the segregation of individual species, the total population density profile, $N_{\mathrm{tot}}(x) = \sum_i N_i(x)$, (dashed line in Fig. 3a–c) remains nearly constant over time, maintaining a smooth, almost linearly declining function across the entire gradient. After 10^4 time steps the growth-specialist,

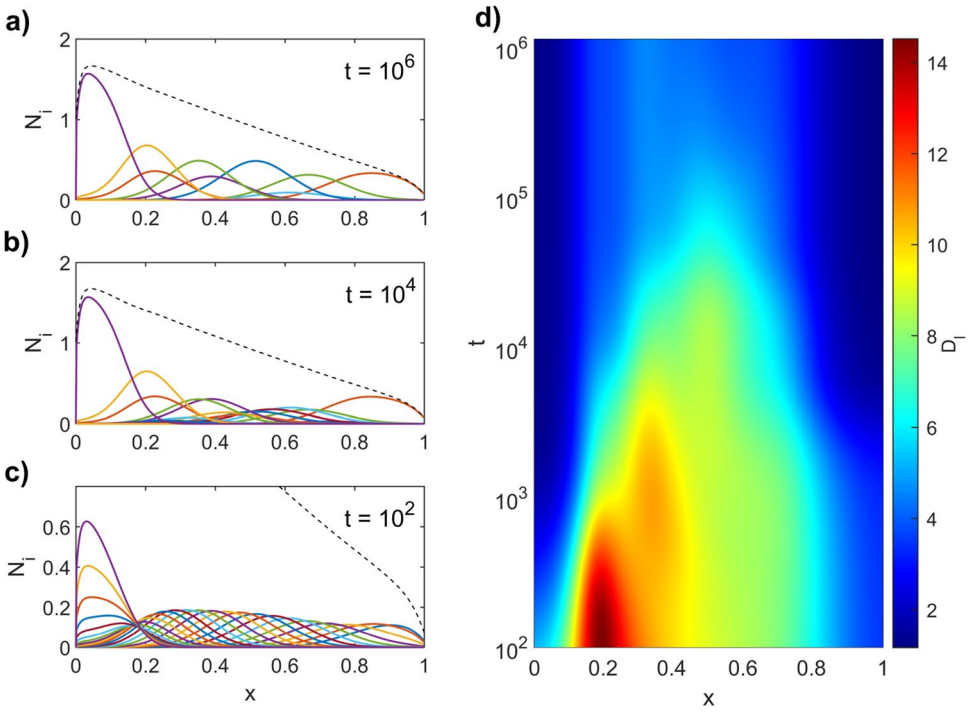

Fig. 3 Community patterns and diversity over extended simulation times for a 25-species community. **a–c** Species density profiles $N_i(x)$ along the stress gradient x after **a** 10^6, **b** 10^4, and **c** 10^2 time steps. Note the different vertical scale in **c**. The total population density N_{tot} is shown by the dashed black line in each panel. The panels (**a–c**) are ordered from the latest time point to the earliest (top to bottom) to align with the temporal diversity patterns shown on the right. **d** Local species richness D_l (indicated by color coding) across the stress gradient x and simulation time t (note the logarithmic axis). The figure has been smoothed using the interpolated shading function, provided by MATLAB. The peak in species richness undergoes two noticeable shifts towards the center of the gradient, where it stabilizes and persists for a prolonged period during the simulation. Parameter values are equivalent to the simulation used in the bottom row of Fig. 2

the species with the highest growth rate R_i (purple line in Fig. 3b) dominates the benign end, reaching a peak density of about 1.6. Further into the gradient ($x \approx 0.1$), the growth-specialist declines in density and other species emerge with moderate maximal densities ranging from 0.3 to 0.6. In the middle of the gradient ($0.4 < x < 0.6$) multiple species coexist at low abundances, with significant overlap in their density curves. The most stressful end ($x > 0.8$) is dominated again by a single species, the stress-tolerant specialist. At this stage, the community has reached a characteristic state with the highest local diversity at intermediate stress levels (Fig. 8).

As the simulation continues over longer time scales, the community enters a period of long transients, with only marginal changes in species composition at each time step. Consequently, it takes about 10^6 time steps to reach a steady state (Fig. 3a). At this steady state, only 9 out of the initial 25 species survive, resulting in reduced overall diversity, although a hump-shaped diversity pattern still persists (Fig. 8l). A closer look at the diversity pattern reveals some intriguing model behavior (Figs. 3d and 9). While, initially ($t < 1000$) the diversity peak is situated near the benign end of the gradient ($x \approx 0.2$), over time, it shifts towards the center of the gradient, including two notable jumps around $t \approx 1000$ and $t \approx 6000$, after which the peak stabilizes at the center of the gradient for the remainder of the simulation. Such rapid changes suggest the occurrence of trait lumping, where species with similar traits cluster in particular regions along the gradient (Scheffer & Nes 2006). When such clusters collapse due to extinction, they can trigger abrupt shifts in the diversity pattern (discussed further below).

Figure 4 offers deeper insights into the mechanisms driving these shifts in diversity pattern, focusing on a larger community of 500 species, with the same evenly distributed trait values as before. The left column of the figure illustrates the temporal development of species presence and extinction over 10^6 time steps. As with the 25-species community, global diversity gradually declines over time as species densities fall below the extinction threshold, leading to their removal from the community. However, these extinctions are not random but clustered

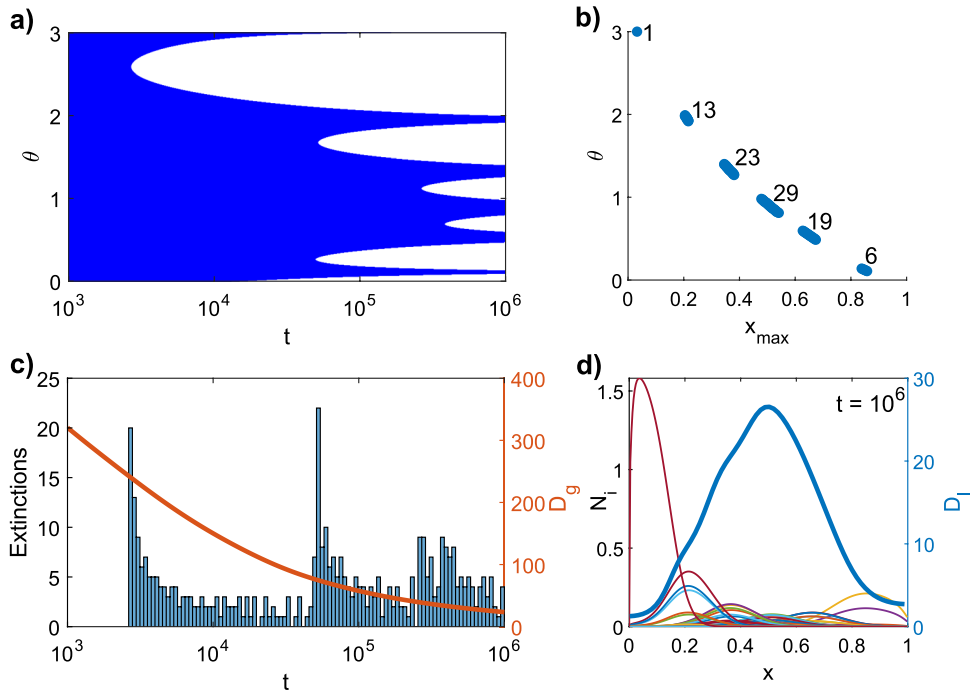

Fig. 4 Formation of trait lumping and diversity profile for a community with 500 species, showing the temporal development of species presence and extinction over 10^6 time steps (left) and community structure at the end of the simulation (right). **a** Species survival based on their trade-off position θ is depicted over simulation time t (note the logarithmic axis). Blue areas represent species that are still present, whereas white areas indicate species that have gone extinct. **b** Clustering of species that survived until the end of the simulation ($t = 10^6$), shown by their trade-off position θ and the spatial location of maximal density, x_{max}. The number beside each cluster indicates how many species are present in that cluster. **c** Histogram of extinction events (using 100 bins, blue bars) across simulation time, alongside global diversity D_g (orange line). The histogram reveals the timing and frequency of extinction events during the simulation. **d** Spatial density profiles $N_i(x)$ (thin lines) and local diversity D_l along the gradient (thick blue line) at $t=10^6$, highlighting the increased diversity towards the center of the gradient

among species with similar trait values, as indicated by species survival times relative to their trait values θ_i (blue-shaded regions in Fig. 4a). These clusters occur in distinct large extinction waves, as indicated by the temporal pattern of extinction rates (blue bars in Fig. 4c). The two largest extinction events took place around $t = 2700$ and $t = 52{,}000$ time steps, followed by smaller but still notable events around $t = 260{,}000$ and $t = 370{,}000$. These waves of extinction coincide with the formation of large trait gaps (white areas in Fig. 4a), indicating the loss of species with similar trait values and leaving behind distinct clusters of surviving species.

Figure 4b shows where these clusters form along the gradient and the trade-off curve, indicated by their positions of maximum density x_{max} and their corresponding trait values θ_i. In general, higher θ values correspond to larger maximal growth rates R_i, while lower θ values are associated with greater stress tolerance T_i. The size and distribution of these clusters vary across the gradient. At the benign end, only a single species—the growth-specialist with the highest θ value—remains by the end of the simulation. Moving towards the center of the gradient, five additional clusters emerge, the largest of these with 29 species located at $x = 0.5$, while at the hostile end, six species survive in the final cluster.

Figure 4d illustrates how these clusters along the trait axis translate into the spatial structure and diversity of the community. The benign end of the gradient is dominated

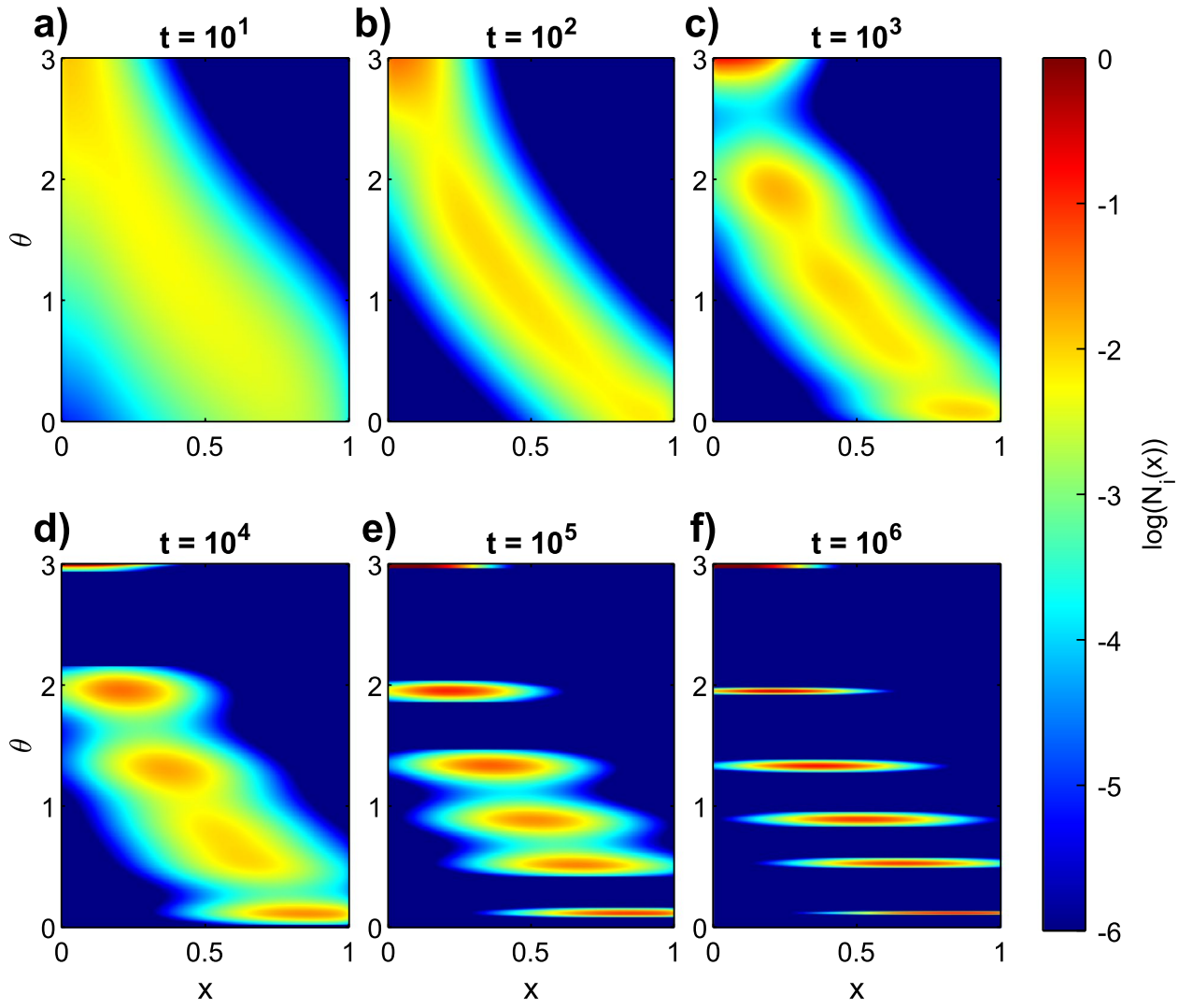

Fig. 5 Temporal development of trait lumping across the spatial gradient. The figure shows the distribution of population densities $N_i(x)$, visualized on a logarithmic scale in color coding, along the gradient x relative to species' trait values θ, at different stages in a 500 species simulation (parameter values as in Fig. 4). Note the narrow density peak close to $\theta = 3$, corresponding to the growth-specialist, that emerges for large simulation times (trait range slightly enlarged in **e** and **f** to make it visible)

by a single species, corresponding to the one-species cluster seen in Fig. 4c, while at the hostile, end two species persist. In intermediate regions, the community exhibits much greater diversity due to the presence of larger species clusters. This creates a hump-shaped diversity distribution that peaks in the middle of the gradient. The spatial aspect of the formation of trait lumping is further illustrated in Fig. 5, which shows the distribution of population densities in space relative to species' trait values. The figure highlights a key distinction in the distribution of simulated population densities across spatial and trait dimensions: as simulation time increases, trait clusters, separated by distinct gaps, form along the trait axis, while spatial ranges of species remain to show substantial overlaps.

Finally, we investigate the impact of dispersal range σ on species patterns, as shown in Figs. 6 and 10, which present long-term community structures and diversity profiles for a community of 25 species under varying dispersal conditions. For reference, Fig. 6b illustrates the results for a medium dispersal range of $\sigma = 0.02$, replicating the outcomes from Fig. 3b and exhibiting a hump-shaped diversity profile centered in the middle of the gradient. In contrast, Fig. 6a illustrates a scenario for a wider dispersal range ($\sigma = 0.05$), where species density profiles are spread more widely across the gradient, and only a small number of species (seven) survive after 10^4 time steps. At the other extreme, Fig. 6c presents the case of a very narrow dispersal range ($\sigma = 0.0005$), where species density curves become much more localized, indicating that each species occupies only a small section of the gradient. At the benign end, a monoculture of the growth-specialist dominates a wide region, followed by a series of species with narrower ranges and lower maximum densities. Species adjacent to the growth-specialist are tightly packed, leading to a peak in local diversity near the boundary of the growth-specialist's range. Interestingly, despite these shifts in individual species density profiles, the total population density profile $N_{tot}(x)$ (dashed lines in Fig. 6a–c) remains largely unaffected by changes in dispersal width.

These results highlight the significant influence of dispersal range σ on both the magnitude and the location of the diversity peak. Figure 6d shows how local diversity changes across the gradient as σ increases. At low σ, the highest local diversity is found near the benign end, albeit with a relatively modest peak of around 4. As σ increases, the diversity peak shifts linearly towards the center of the gradient, accompanied by a notable rise in magnitude, with local effective species richness reaching levels up to 9 (visible as a red wedge, indicating high local diversity, in the lower left corner of Fig. 6d). However, once the diversity peak has reached the center of the gradient at $\sigma = 0.02$, further increases in dispersal range lead to no clear changes in diversity patterns. This likely reflects ongoing species extinctions triggered when critical dispersal thresholds are passed, causing non-monotonic behavior in species density and diversity profiles.

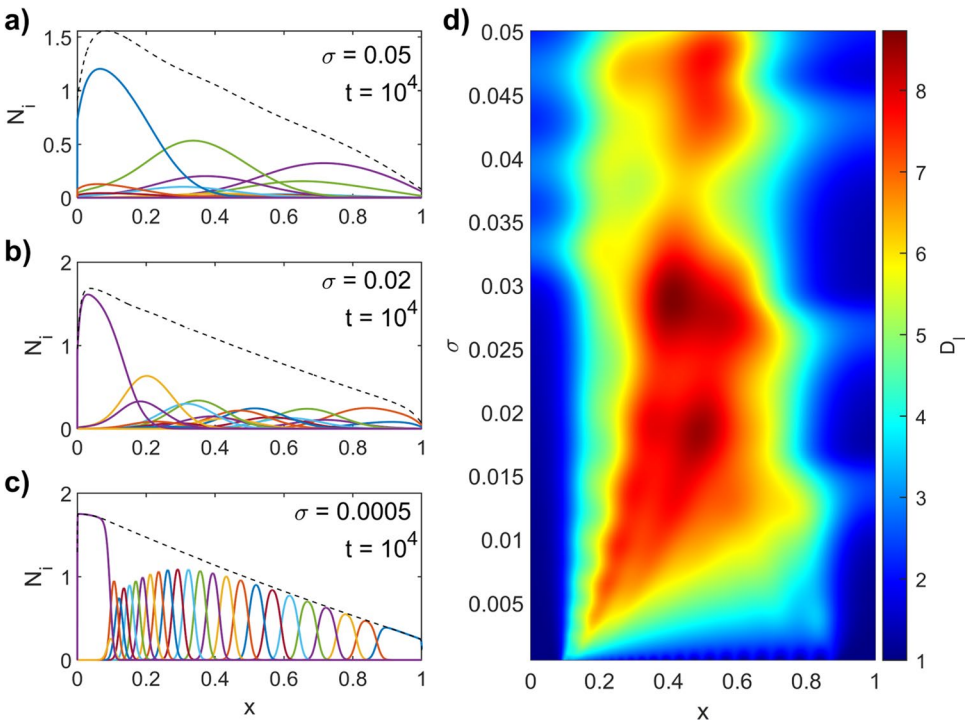

Fig. 6 Influence of dispersal kernel width σ on spatial community patterns and diversity for a community with 25 species. **a**–**c** Species density profiles $N_i(x)$ along the spatial gradient x are shown after 10^4 time steps for three different dispersal widths: **a** large, $\sigma = 0.05$; **b** intermediate, $\sigma = 0.02$; and **c** small, $\sigma = 0.0005$. The total population density N_{tot} is shown by the dashed black line in each panel. **d** Local species richness D_l (indicated by color coding) across the stress gradient x and the dispersal width σ (smoothing as in Fig. 3). The peak in diversity shifts towards the center of the gradient as σ increases. At higher dispersal rates, diversity significantly decreases

Discussion

Traditionally, niche-based models of distinct preferences assume that species achieve their optimal performance at different positions along a spatial or environmental gradient (Rosenzweig 1991; Violle and Jang, 2009; Anderson et al. 2022). In contrast, here we adopted an alternative model of shared preferences, where all species reach their highest intrinsic growth rates at the benign, low-stress end of the gradient (Rosenzweig 1991; Wisheu 1998; McGill et al. 2006). Coexistence is maintained by a growth-tolerance trade-off, representing different adaptations of species to tolerate stress. This creates a clear niche differentiation, where each species achieves its highest growth rate within a specific region along the gradient where it can dominate all others (Fig. 1g). Growth-specialists dominate the benign regions of the gradient, while more tolerant species are best adapted to the hostile end of the gradient, where they can locally achieve the highest growth rates. In sum, this creates a competitive hierarchy, in which each species can outgrow the others in specific regions dictated by its rank in the growth-tolerance hierarchy (Keddy et al. 2000; Gross et al., 2014; Pfestorf et al. 2016). This pattern is reflected in our numerical simulations: despite having their performance peaks at the benign end of the gradient, all species are confined to narrow environmental ranges and sorted into a pattern of spatially segregated, but overlapping unimodal density profiles (Figs. 2 and 3). This outcome, typically associated with distinct species preferences (Whittaker 1967a, b), was achieved here for a community with shared preferences, independent of initial conditions.

The emerging spatial profiles are, however, not dictated by abiotic requirements alone. Community structure is defined by a combination of factors, including dispersal and species interactions (Thompson et al. 2020). Most dominantly, dispersal mixes regions of local dominance, intensifying competitive interactions and reducing species densities, which may trigger competitive exclusion. Thus, after the ready establishment of species segregation within a relatively short time span (Fig. 2), over longer time scales species ranges are modified due to ongoing interactions. This leads to long-term temporal shifts and reorganization of the spatial community structure (Fig. 3). Similar long times to reach equilibrium have been observed in other models of communities on spatial gradients (Mohammed et al. 2022). The origin of these long transients can be explained by diminishing fitness differences as species adapt and shift their local ranges. Consequently, the time required for slightly more fit species, or groups of species, to locally outcompete their neighbors increases, leading to slower rates of competitive displacement and local extinction. In total, this process stabilizes species configurations, resembling to a "freezing" process where community structure becomes increasingly stable with time.

This slow transition, however, is punctuated by extinction events in which species in whole regions along the trade-off curve go extinct. As demonstrated in Fig. 4a, these extinctions go together with spatial shifts in the peak of local diversity towards the middle of the gradient and the formation of trait lumping. The first wave of extinctions affects species with high θ_i values (species favoring growth over tolerance), dominating regions close to the benign end of the gradient. These extinctions are driven by the strong competition from the growth-specialist. This species plays a pivotal role in this process as it benefits from two effects: first, from having its dominance in a region where it also achieves its maximum intrinsic growth, and second from the boundary conditions, as it is influenced by propagule pressure only from a single side. As a result, it is able to establish high densities in the benign region and spread large amounts of propagules into neighboring areas. Eventually, the dispersal pressure from the growth-specialist becomes too large, and adjacent species with narrow dominance regions are unable to sustain their population and go extinct. This results in an extinction wave, creating a gap in the trait distribution. Notably, the change in local diversity occurs before these extinction events, as our diversity measure (derived from the Shannon index) can detect changes in the distribution of local abundances before extinction takes place. While this extinction event negatively impacts species in the benign end, it has a beneficial influence on species that are located next to the extinction zone, as it reduces competitive pressure, temporally increasing local biodiversity in this area. Consequently, the diversity peak shifts towards the middle of the gradient.

A further result of these processes is the formation of trait lumping (Scheffer & van Nes 2006), that is, the emergence of clusters of species with similar trait values (Fig. 4). The resulting trait-lumping patterns along the gradient (Fig. 5) resemble those observed in other spatially explicit models (Doebeli and Dieckmann 2003; Leimar et al. 2008; Norberg et al. 2012; Mohammed et al. 2022). However, to our knowledge, this is the first time that trait lumping has been demonstrated to occur in time-discrete systems and in a gradient with shared preferences. Unlike the well-known trait-lumping mechanism (Scheffer & van Nes 2006), which arises from a genuine pattern-formation process (Pigolotti et al. 2007), in our model, trait lumping is driven by the boundary conditions at the benign end of the gradient. These

favor the dominance of the growth-specialist, leading to the subsequent extinction of adjacent species. Species located farther from the influence of the growth-specialist are less impacted by dispersal pressure and benefit from the extinction of nearby species. This creates a cascading effect, where species exert competitive pressure on their neighbors, leading to further extinctions and creating clusters of surviving species. Cluster sizes vary along the gradient, with smaller clusters near the benign end due to the intense competition, larger clusters at intermediate stress, and subsequently smaller clusters near the hostile end due to strong environmental filtering.

One of the most notable outcomes of our model is the formation of a characteristic unimodal diversity distribution along the gradient. This pattern aligns with the general theory for the formation of unimodal diversity patterns along stress gradients (Grime 1973). According to this theory, diversity peaks arise from the combination of two distinct processes at the two ends of the gradient: intense competition at the benign end, leading to the exclusion of species, and harsh conditions at the stressful end, which restrict species survival. Together, these processes create a diversity maximum in the middle of the domain. This unimodal diversity pattern is reminiscent to the mid-domain effect, which posits that diversity tends to be higher in the middle of a spatial domain, even in the absence of environmental gradients (Colwell & Lees, 2000; Prillwitz & Blasius 2020). To test whether the mid-domain contributed to our results, we conducted a simulation where the gradient was mirrored, creating benign conditions in the middle and hostile conditions on both ends (Fig. 11). The simulation produced a bimodal diversity distribution, with two diversity peaks at intermediate stress levels. This finding confirms that, contrary to the mid-domain effect, it is not merely the distance to the boundaries that drives the diversity peak, but rather the intensity of the stress along the gradient.

Even though our model is designed primarily as a conceptual framework, the resulting diversity distributions closely resemble pattern observed in various ecosystems characterized by a stress gradient (e.g., Sousa 1979; Grytnes & Vetaas 2002). Perhaps the most striking comparison can be made with salt marsh ecosystems. In salt marshes, clear stress gradients are created by variations in salinity and flooding frequency, both of which have a strong negative effect on plant growth (Crain et al. 2004; Veldhuis et al. 2019). Consistent with our model predictions, the upper salt marsh, where stress is minimal, is often dominated by a single species. In contrast, the lower salt marsh, where stress levels are moderate, supports a high diversity of plant species. Finally, in the pioneer zone, where the salinity and inundation frequency are at its maximum, only a few highly stress-tolerant species can survive at low densities (Pennings & Bertness 2001; Bauer et al. 2021). These three distinct zones of varying diversity levels mirror transient patterns observed in our model. Moreover, several empirical studies have shown that species typically found in high-stress zones of salt marshes exhibit better performance when transplanted into more benign environments (Pennings et al. 2005; Engels & Jensen 2010). This observation supports our model's core assumption: all species, regardless of where they are found along the stress gradient, achieve their optimal performance under conditions of minimal stress.

While our conceptual study captures essential aspects of natural ecosystems along stress gradients, some biologically relevant factors were simplified or left out, offering numerous avenues for extensions and future research. One key area for future investigation is a closer examination of competitive interactions. We assumed identical competition coefficients between all species. It would be valuable to explore how varying intra- and interspecific competition coefficients, α_{ij}, possibly in relation to species' trait values, impact community dynamics. Although parameterizing these coefficients from empirical data is challenging, doing so would offer a more nuanced understanding of competition dynamics. Another potential extension could involve incorporating additional trade-offs, such as a competition-colonization trade-off that relates growth or competitive abilities with dispersal strength (Kneitel & Chase 2004).

Moreover, it would be intriguing to explore how model results are influenced by the analytical form of the used response functions. For instance, the spatial growth rate function $r_i(x)$ (Eq. (4)) and the trade-off curve (Eqs. (5) and (6)) could be varied. Our numerical tests with alternative spatially decaying growth rate functions and different trade-off curves (by varying the shape parameters β) suggest that our main results remain unchanged as long as the most tolerant species can still survive and outcompete others on the hostile end of the gradient. Another interesting option for future research is to expand the model, for example by introducing trophic interactions, such as a consumer species preying on the most abundant species ("kill-the-winner" dynamics), which could substantially alter the model outcome by reducing the dominance of growth-specialists and promoting predator-mediated coexistence (Caswell 1978). Similarly, incorporating the feedback of species on their abiotic environment, akin to the process of niche construction (e.g., sedimentation processes in salt marshes), could provide new insights by allowing species to modify, and potentially ameliorate, stress levels in their habitats. Another intriguing model

extension would be to investigate communities on environmental gradients that still exhibit a growth-tolerance trade-off, but in which the position of maximal growth is not identical for all species.

In our simulations, we intentionally kept the maximum growth rate R_{max} sufficiently low enough to avoid period-doubling bifurcations. However, it would be theoretically interesting to explore the model in an oscillatory regime, as this could reveal how diversity patterns are influenced by oscillations and whether these patterns depend on the synchrony of density fluctuations at different points along the gradient. Additionally, expanding the spatial scale of the model, by adding a second dimension to the gradient or simulating a network of multiple interconnected patches (Thompson et al. 2020) could yield further insights.

Our analysis identified long-term changes in community structure in a stationary environment, undergoing temporal changes over millions of generations even for small communities. The timescales that it takes in the model to reach a steady state with low diversity suggest that in nature, it would be unlikely that an ecosystem will ever reach such states, as it would require a constant environment for an extremely long time. This raises the question whether stress gradients in nature may be present in the transient rather than the final steady states of our simulations. These ideas can be explored in further studies which could incorporate environmental variability by introducing stochastic disturbances, such as fluctuating model parameters or species invasions. Preliminary tests, where we coupled the model with immigration from an external species pool (i.e., sampling invaders randomly from the trade-off curve), retained unimodal diversity maxima. Moreover, varying the timing of species arrivals produced patterns reminiscent of those shown in Fig. 3a–c. These early simulations suggest that a homogeneously filled trade-off curve under stable conditions can mimic the long-term patterns seen in a system subjected to repeated perturbations.

In conclusion, the model presented in this study provides a flexible framework for investigating the processes and patterns that shape metacommunities across spatial gradients. Our simulations present a picture of metacommunities along stress gradients as a system that is characterized by extremely long transients and complex dynamic outcomes, such as lumping of trait values and punctuated extinctions. Why then is the notion of shared preferences, or inclusive niches, so underrepresented in theoretical ecology? One possible explanation may be the implicit assumption that the distribution of species in nature should mirror their fundamental niches, meaning that observed range limits should align with niche boundaries and areas of high abundances indicate optimal or near-optimal growth conditions. At first glance, community structured by inclusive niches would seem to violate this principle. In such systems, species are often observed in regions with suboptimal conditions, far from their fundamental niche. Here, we have shown that a growth-tolerance trade-off naturally leads to such an outcome where species are pushed into less favorable regions due to competition, resulting in spatial zonation patterns that resemble those obtained from the concept of distinct preferences. This contradiction, where high abundance does not necessarily equate to optimal performance, challenges traditional models of species distribution. Our findings highlight the importance of growth-tolerance trade-offs and provide insight into the complexity of community organization along stress gradients. By bringing attention to this overlooked dynamic, we aim to encourage further exploration of shared preferences in ecological models.

Appendix

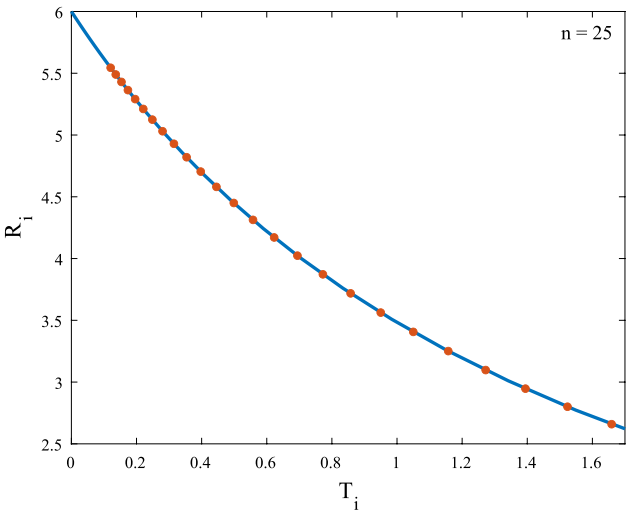

Fig. 7 Trait-positions in the 25-species community. The figure illustrates the position of each species along the trade-off curve (blue line) within the 25-species community, showing their respective tolerance T_i and maximal growth rate R_i (red circles). Even though trait values θ_i are evenly spaced, due to the nonlinearity of Eqs. (5) and (6), the resulting pairwise distances along the trade-of curve are increasing for more tolerant species (from left to right in the figure)

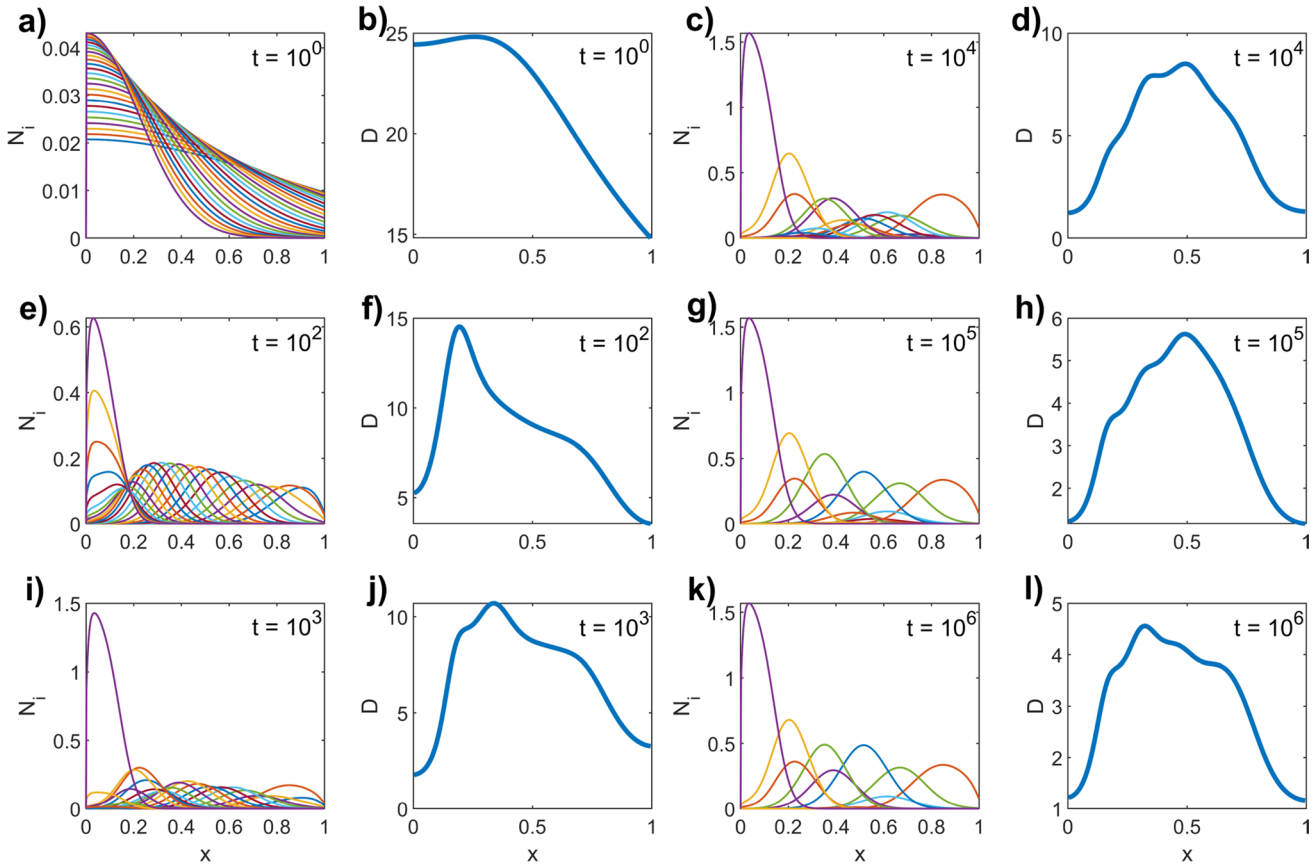

Fig. 8 Temporal development of spatial profiles and diversity over extended time periods. The panels show species density $N_i(x)$ and the corresponding local species richness D_l(thick blue lines) for a community of 25 species (parameter values as in the bottom row of Fig. 2) along the gradient at six different time points, ranging from **a**, **b** $t = 10^0$ to **k**, **l** $t=10^6$. All species start with a small, homogeneously distributed initial density. As the time progresses, the peak in diversity shifts from the benign end of the gradient towards intermediate levels of stress

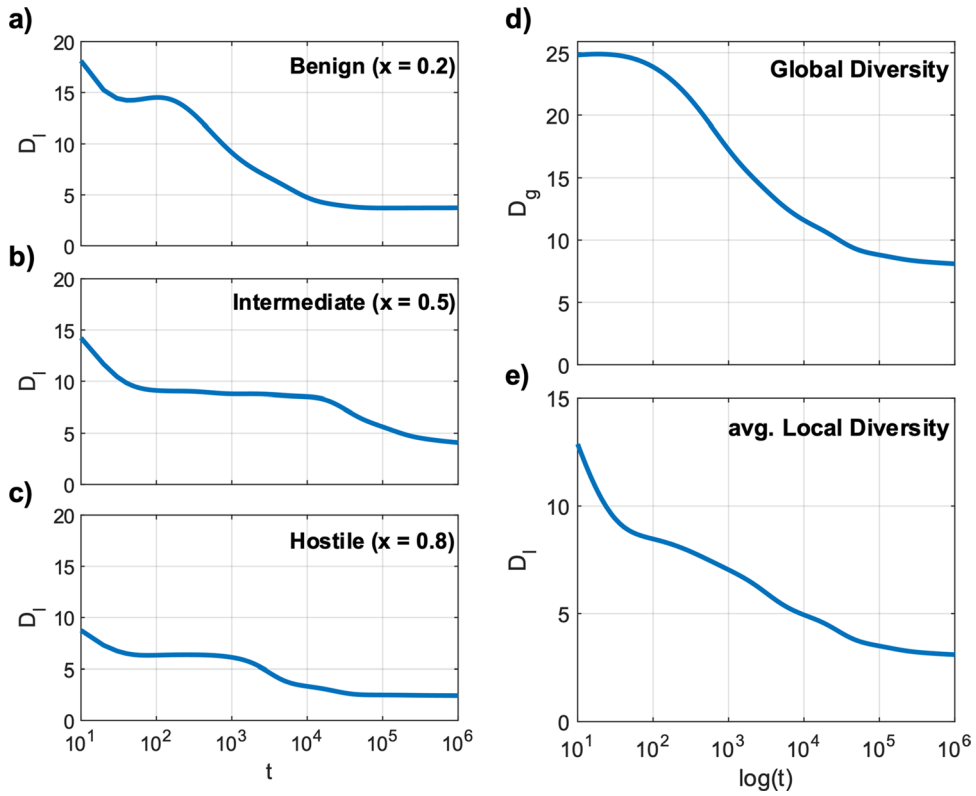

Fig. 9 Temporal development of diversity in a community of 25 species. **a**–**c** Local diversity D_l as a function of time t at different positions along the gradient at **a** benign ($x=0.2$), **b** intermediate ($x=0.5$), and **c** hostile ($x=0.8$) stress levels. **d** Global diversity D_g and **e** average local diversity D_l of the community as a function of time. Parameter values as in the bottom row of Fig. 2. The panels illustrate that during the first phase of the simulation, local diversity is highest at the benign end (**a**). However, after approximately 100 time steps, local diversity declines rapidly, dropping from $D_l = 15$ to $D_l = 4$ at $t = 10^4$, where it remains until the end of the simulation. At intermediate stress levels (**b**), local diversity also declines quickly within the first 50 time steps, stabilizing around $D_l = 9$ until a second drop to $D_l = 4$ occurs at about $t = 2 * 10^4$. At the hostile end of the gradient (**c**), diversity is lowest overall, decaying in two steps at $t = 50$ and $t = 2 * 10^3$, ultimately reaching a final level of $D_l = 2.5$. The right-hand column illustrates that both global diversity and averaged local diversity show an ongoing decline over time until the system reaches a stationary state. Initially, averaged local diversity decreases rapidly within the first 50 simulation time steps, reflecting early spatial shifts in species ranges. In contrast, global diversity remains relatively stable until about $t = 100$, at which point many species start to decline in density, eventually leading to extinction. Overall, these findings show that diversity at intermediate stress levels persists much longer compared to the benign or hostile ends, and that the decline in diversity is not continuous but punctuated by abrupt drops, corresponding to the extinction of groups of species

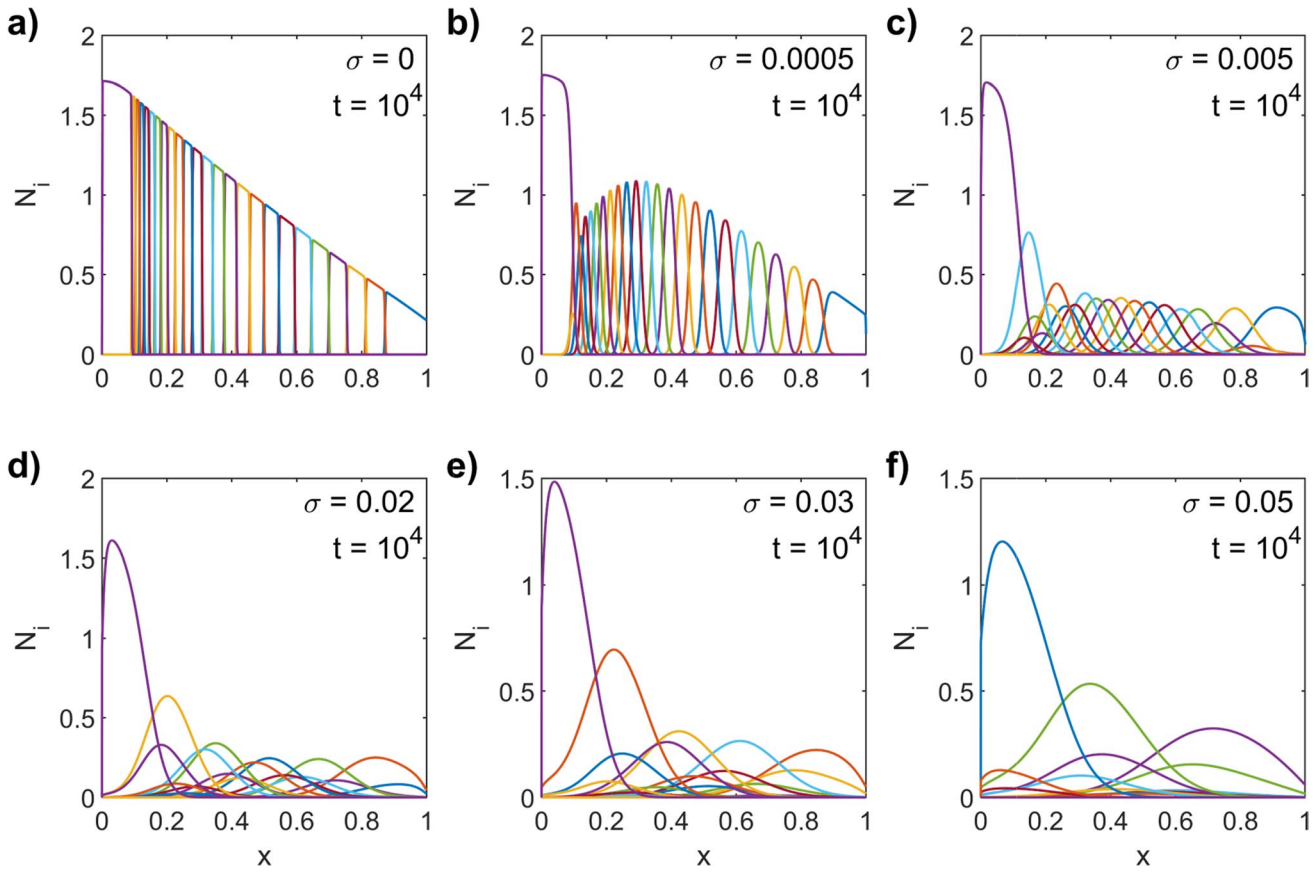

Fig. 10 Community patterns as a function of dispersal width σ. The figure shows simulated density profiles $N_i(x)$ in a community of 25 species after 10^4 time steps for different value of σ, ranging from **a** no dispersal ($\sigma = 0$) to **f** high ($\sigma = 0.05$) dispersal width. In this absence of dispersal **a**, local scale coexistence is not possible under our standard parameterization $\alpha_{ij} = 1$. Instead, each species is able to outcompete the rest of the community within the area where it has the highest growth rate, with overall densities declining linearly from the benign to the hostile end - similar to the total abundance trend observed with positive dispersal (dashed lines in Fig. 6 a–c). As dispersal increases, local coexistence emerges driven by source-sink dynamics, while species density curves remain strongly localized. Additionally, a pronounced dominance of the growth-specialist over the next species in the trade-off curve becomes evident

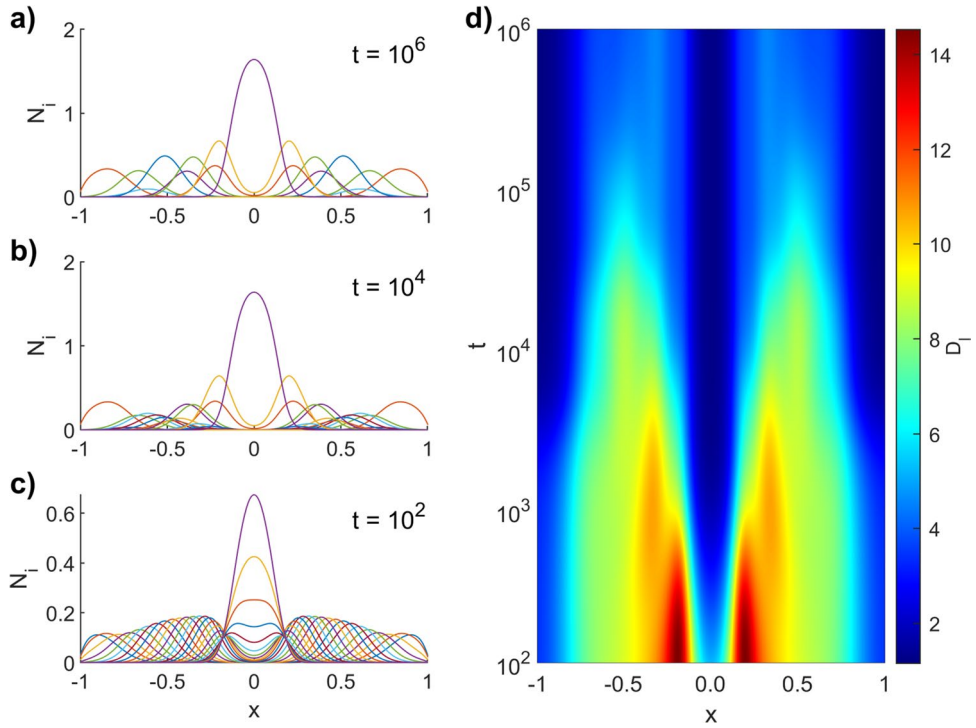

Fig. 11 Influence of boundary conditions on community and diversity patterns. The figure shows species distribution profiles and local diversity over extended simulation times for a community of 25 species, following the setup in Fig. 3 but with modified boundary conditions. In this scenario, the spatial range of the gradient has been extended to the interval $-1 \leq x \leq 1$ Unlike in Fig. 3 and the standard setup, where the gradient terminates at a low-stress boundary, this simulation continuous into a second region of more stressful conditions (for negative values of x), effectively creating a mirrored gradient. Thereby, the previously closed boundary at $x = 0$ has been replaced with a permeable transition, where stress conditions reverse as x decreases to the left. The characteristic pattern of highest diversity at intermediate stress levels, and its temporal shifts, is replicated on both sides of the gradient, confirming that these patterns are not artifacts of the boundary conditions

Acknowledgements We thank Michael Kleyer, James McLaren, and Alexey Ryabov for useful comments on the manuscript.

Author contribution Bernd Blasius conceived the idea, Torben Schucht conducted the numerical simulations and wrote the original draft, both authors contributed to the interpretation of results, and the writing and editing of the manuscript.

Funding Open Access funding enabled and organized by Projekt DEAL. This project was funded by the Deutsche Forschungsgemeinschaft (DFG, German Research Foundation), within the project DynaCom (FOR 2716)—Projektnummer 379417748.

Data Availability No datasets were generated or analysed during the current study.

Code availability The software code of the numerical model that has been used to generate the is publicly results and the figures available from the research repository Zenodo: https://doi.org/10.5281/zenodo.14163043.

Declarations

Competing interests The authors declare no competing interests.

References

Andersen M (1991) Properties of some density-dependent integrodifference equation population models. Math Biosci 104(1):135–157. https://doi.org/10.1016/0025-5564(91)90034-G

Anderson MJ, Walsh DCI, Sweatman WL, Punnett AJ (2022) Nonlinear models of species' responses to environmental and spatial gradients. Ecol Lett 25(12):2739–2752. https://doi.org/10.1111/ele.14121

Anten NPR, Hirose T (1999) Interspecific differences in above-ground growth patterns result in spatial and temporal partitioning of light among species in a tall-grass meadow. J Ecol 87(4):583–597. https://doi.org/10.1046/j.1365-2745.1999.00365.x

Arribas P, Gutiérrez-Cánovas C, Botella-Cruz M, Cañedo-Argüelles M, Antonio Carbonell J, Millán A, Pallarés S, Velasco J, Sánchez-Fernández D (2019) Insect communities in saline waters consist of realized but not fundamental niche specialists. Philos Trans R Soc B 374(1764):20180008. https://doi.org/10.1098/rstb.2018.0008

Bauer B, Kleyer M, Albach DC, Blasius B, Brose U, Ferreira-Arruda T, Feudel U, Gerlach G, Hof C, Kreft H, Kuczynski L, Lõhmus K, Moorthi S, Scherber C, Scheu S, Zotz G, Hillebrand H (2021) Functional trait dimensions of trophic metacommunities. Ecography 44(10):1486–1500. https://doi.org/10.1111/ecog.05869

Caswell H (1978) Predator-mediated coexistence: a nonequilibrium model. Am Nat 112(983):127–154. https://doi.org/10.1086/283257

Colwell RK, Lees DC (2000) The mid-domain effect: geometric constraints on the geography of species richness. Trends in Ecology & Evolution 15(2):70–76. https://doi.org/10.1016/S0169-5347(99)01767-X

Colwell RK, Fuentes ER (1975) Experimental studies of the niche. Annu Rev Ecol Syst 6:281–310. https://doi.org/10.1146/annurev.es.06.110175.001433

Crain CM, Silliman BR, Bertness SL, Bertness MD (2004) Physical and biotic drivers of plant distribution across estuarine salinity gradients. Ecology 85(9):2539–2549. https://doi.org/10.1890/03-0745

D'Andrea R, Barabás G, Ostling A (2013) Revising the tolerance-fecundity trade-off; or, on the consequences of discontinuous resource use for limiting similarity, species diversity, and trait dispersion. Am Nat 181(4):E91–E101. https://doi.org/10.1086/669902

D'Andrea R, O'Dwyer JP (2021) Competition for space in a structured landscape: the effect of seed limitation on coexistence under a tolerance-fecundity trade-off. Journal of Ecology 109(4):1886–1897. https://doi.org/10.1111/1365-2745.13613

D'Andrea R, Riolo M, Ostling AM (2019) Generalizing clusters of similar species as a signature of coexistence under competition. PLoS Comput Biol 15(1):e1006688. https://doi.org/10.1371/journal.pcbi.1006688

Delfau J-B, Ollivier H, López C, Blasius B, Hernández-García E (2016) Pattern formation with repulsive soft-core interactions: discrete particle dynamics and Dean-Kawasaki equation. Phys Rev E 94(4):042120. https://doi.org/10.1103/PhysRevE.94.042120

Doebeli M, Dieckmann U (2003) Speciation along environmental gradients. Nature 421(6920):259–264. https://doi.org/10.1038/nature01274

Engels JG, Jensen K (2010) Role of biotic interactions and physical factors in determining the distribution of marsh species along an estuarine salinity gradient. Oikos 119(4):679–685. https://doi.org/10.1111/j.1600-0706.2009.17940.x

Gauch HG, Whittaker RH (1972) Coenocline simulation. Ecology 53(3):446–451. https://doi.org/10.2307/1934231

Grime JP (1973) Competitive exclusion in herbaceous vegetation. Nature 242(5396):344–347. https://doi.org/10.1038/242344a0

Gross N, Liancourt P, Butters R, Duncan RP, Hulme PE (2015) Functional equivalence, competitive hierarchy and facilitation determine species coexistence in highly invaded grasslands. New Phytol 206(1):175–186. https://doi.org/10.1111/nph.13168

Grytnes JA, Vetaas OR (2002) Species richness and altitude: a comparison between null models and interpolated plant species richness along the Himalayan altitudinal gradient. Nepal the American Naturalist 159(3):294–304. https://doi.org/10.1086/338542

Guo Q, Kelt DA, Sun Z, Liu H, Hu L, Ren H, Wen J (2013) Global variation in elevational diversity patterns. Sci Rep 3(1):3007. https://doi.org/10.1038/srep03007

Hutchinson GE (1957) Concluding remarks. Cold Spring Harb Symp Quant Biol 22:415–427. https://doi.org/10.1101/SQB.1957.022.01.039

Jaszczuk I, Kotowski W, Kozub Ł, Kreyling J, Jabłońska E (2023) Physiological responses of fen mosses along a nitrogen gradient point to competition restricting their fundamental niches. Oikos 2023(2):e09336. https://doi.org/10.1111/oik.09336

Jost L (2006) Entropy and diversity. Oikos 113(2):363–375. https://doi.org/10.1111/j.2006.0030-1299.14714.x

Keddy P, Gaudet C, Fraser LH (2000) Effects of low and high nutrients on the competitive hierarchy of 26 shoreline plants. J Ecol 88(3):413–423. https://doi.org/10.1046/j.1365-2745.2000.00456.x

Kim D, Ohr S (2020) Coexistence of plant species under harsh environmental conditions: an evaluation of niche differentiation and stochasticity along salt marsh creeks. Journal of Ecology and Environment 44(1):19. https://doi.org/10.1186/s41610-020-00161-y

Kneitel JM, Chase JM (2004) Trade-offs in community ecology: linking spatial scales and species coexistence. Ecol Lett 7(1):69–80. https://doi.org/10.1046/j.1461-0248.2003.00551.x

Körner, C. (2007). The use of 'altitude' in ecological research. *Trends in Ecology & Evolution*, *22*(11), 569–574. https://https://doi.org/10.1016/j.tree.2007.09.006

Leibold MA (1998) Similarity and local co-existence of species in regional biotas. Evol Ecol 12(1):95–110. https://doi.org/10.1023/A:1006511124428

Leibold MA, Holyoak M, Mouquet N, Amarasekare P, Chase JM, Hoopes MF, Holt RD, Shurin JB, Law R, Tilman D, Loreau M, Gonzalez A (2004) The metacommunity concept: a framework for multi-scale community ecology. Ecol Lett 7(7):601–613. https://doi.org/10.1111/j.1461-0248.2004.00608.x

Leibold MA, Chase JM, Ernest SKM (2017) Community assembly and the functioning of ecosystems: how metacommunity processes alter ecosystems attributes. Ecology 98(4):909–919. https://doi.org/10.1002/ecy.1697

Leimar O, Doebeli M, Dieckmann U (2008) Evolution of phenotypic clusters through competition and local adaptation along an environmental gradient. Evolution 62(4):807–822. https://doi.org/10.1111/j.1558-5646.2008.00334.x

Letten AD, Ke P-J, Fukami T (2017) Linking modern coexistence theory and contemporary niche theory. Ecol Monogr 87(2):161–177. https://doi.org/10.1002/ecm.1242

Loehle C (1998) Height growth rate tradeoffs determine northern and southern range limits for trees. J Biogeogr 25(4):735–742. https://doi.org/10.1046/j.1365-2699.1998.2540735.x

Lutscher F (2019) *Integrodifference Equations in Spatial Ecology* (Vol. 49). Springer International Publishing. https://doi.org/10.1007/978-3-030-29294-2

MacArthur R, Levins R (1967) The limiting similarity, convergence, and divergence of coexisting species. Am Nat 101(921):377–385. https://doi.org/10.1086/282505

MacArthur RH, Diamond JM, Karr JR (1972) Density compensation in Island Faunas. Ecology 53(2):330–342. https://doi.org/10.2307/1934090

Mcgill B, Enquist B, Weiher E, Westoby M (2006) Rebuilding community ecology from functional traits. Trends Ecol Evol 21(4):178–185. https://doi.org/10.1016/j.tree.2006.02.002

Mittelbach GG, Steiner CF, Scheiner SM, Gross KL, Reynolds HL, Waide RB, Willig MR, Dodson SI, Gough L (2001) What is the observed relationship between species richness and productivity? Ecology 82(9):2381–2396. https://doi.org/10.1890/0012-9658(2001)082[2381:WITORB]2.0.CO;2

Mohammed M, Blasius B, Ryabov A (2022) Coexistence patterns and diversity in a trait-based metacommunity on an environmental gradient. Thyroid Res 15(1):51–63. https://doi.org/10.1007/s12080-021-00526-6

Muller-Landau HC (2010) The tolerance–fecundity trade-off and the maintenance of diversity in seed size. Proc Natl Acad Sci 107(9):4242–4247. https://doi.org/10.1073/pnas.0911637107

Mumladze L, Shetekaur S, Barnaveli N, Chelidze D, Asanidze Z (2023) Species elevational richness gradient and species-area relationship in mountain vegetation of Javakheti highland (Georgia). Caucasiana 2:127–135. https://doi.org/10.3897/caucasiana.2.e103599

Norberg J, Urban MC, Vellend M, Klausmeier CA, Loeuille N (2012) Eco-evolutionary responses of biodiversity to climate change. Nature Climate Change 2(10):10. https://doi.org/10.1038/nclimate1588

Pennings SC, Bertness MD (2001) Salt marsh communities. *Marine*. Community Ecol 11:289–316

Pennings SC, Grant MB, Bertness MD (2005) Plant zonation in low-latitude salt marshes: disentangling the roles of flooding, salinity and competition. J Ecol 93(1):159–167. https://doi.org/10.1111/j.1365-2745.2004.00959.x

Pfestorf H, Körner K, Sonnemann I, Wurst S, Jeltsch F (2016) Coupling experimental data with individual-based modelling reveals differential effects of root herbivory on grassland plant co-existence along a resource gradient. J Veg Sci 27(2):269–282. https://doi.org/10.1111/jvs.12357

Pigolotti S, López C, Hernández-García E (2007) Species clustering in competitive Lotka-Volterra models. Phys Rev Lett 98(25):258101. https://doi.org/10.1103/PhysRevLett.98.258101

Powell J (2001) Spatio-temporal models in ecology: an introduction to integro-difference equations. Utah State University, Logan (UT)

Ricker WE (1954) Stock and recruitment. J Fish Res Board Can 11(5):559–623. https://doi.org/10.1139/f54-039

Rosenzweig ML (1991) Habitat selection and population interactions: the search for mechanism. Am Nat 137:S5–S28. https://doi.org/10.1086/285137

Sakavara A, Tsirtsis G, Roelke DL, Mancy R, Spatharis S (2018) Lumpy species coexistence arises robustly in fluctuating resource environments. Proc Natl Acad Sci 115(4):738–743. https://doi.org/10.1073/pnas.1705944115

Schamp BS, Chau J, Aarssen LW (2008) Dispersion of traits related to competitive ability in an old-field plant community. J Ecol 96(1):204–212. https://doi.org/10.1111/j.1365-2745.2007.01328.x

Scheffer M, van Nes EH (2006) Self-organized similarity, the evolutionary emergence of groups of similar species. Proc Natl Acad Sci 103(16):6230–6235. https://doi.org/10.1073/pnas.0508024103

Snow AA, Vince SW (1984) Plant zonation in an Alaskan salt marsh: II. An experimental study of the role of edaphic conditions. The Journal of Ecology 72(2):669–684. https://doi.org/10.2307/2260075

Sousa WP (1979) Disturbance in marine intertidal boulder fields: the nonequilibrium maintenance of species diversity. Ecology 60(6):1225–1239. https://doi.org/10.2307/1936969

Suchrow S, Jensen K (2010) Plant species responses to an elevational gradient in German North Sea Salt Marshes. Wetlands 30(4):735–746. https://doi.org/10.1007/s13157-010-0073-3

Telesh I, Schubert H, Skarlato S (2013) Life in the salinity gradient: discovering mechanisms behind a new biodiversity pattern. Estuar Coast Shelf Sci 135:317–327. https://doi.org/10.1016/j.ecss.2013.10.013

Thompson PL, Guzman LM, De Meester L, Horváth Z, Ptacnik R, Vanschoenwinkel B, Viana DS, Chase JM (2020) A process-based metacommunity framework linking local and regional scale community ecology. Ecol Lett 23(9):1314–1329. https://doi.org/10.1111/ele.13568

Tittes SB, Walker JF, Torres-Martínez L, Emery NC (2019) Grow where you thrive, or where only you can survive? An analysis of performance curve evolution in a clade with diverse habitat affinities. Am Nat 193(4):530–544. https://doi.org/10.1086/701827

Veldhuis ER, Schrama M, Staal M, Elzenga JTM (2019) Plant stress-tolerance traits predict salt marsh vegetation patterning. Front Mar Sci 5:501. https://doi.org/10.3389/fmars.2018.00501

Violle C, Jiang L (2009) Towards a trait-based quantification of species niche. Journal of Plant Ecology 2(2):87–93. https://doi.org/10.1093/jpe/rtp007

von Prillwitz K, Blasius B (2020) Mid-domain effect for food chain length in a colonization–extinction model. Thyroid Res 13(3):301–315. https://doi.org/10.1007/s12080-020-00454-x

Wellborn GA, Skelly DK, Werner EE (1996) Mechanisms creating community structure across a freshwater habitat gradient. Annu Rev Ecol Syst 27(1):337–363. https://doi.org/10.1146/annurev.ecolsys.27.1.337

Whittaker RH (1967a) Gradient Analysis of Vegetation 42:207–264. https://doi.org/10.1111/j.1469-185x.1967.tb01419.x

Whittaker RH (1967b) Gradient analysis of vegetation. Biol Rev 42(2):207–257. https://doi.org/10.1111/j.1469-185X.1967.tb01419.x

Wickman J, Diehl S, Blasius B, Klausmeier CA, Ryabov AB, Brännström Å (2017) Determining selection across heterogeneous landscapes: a perturbation-based method and its application to modeling evolution in space. Am Nat 189(4):381–395. https://doi.org/10.1086/690908

Wilson DS (1992) Complex interactions in metacommunities, with implications for biodiversity and higher levels of selection. Ecology 73(6):1984–2000. https://doi.org/10.2307/1941449

Wisheu IC (1998) How organisms partition habitats: different types of community organization can produce identical patterns. Oikos 83(2):246. https://doi.org/10.2307/3546836

Zwerschke N, Bollen M, Molis M, Scrosati RA (2013) An environmental stress model correctly predicts unimodal trends in overall species richness and diversity along intertidal elevation gradients. Helgol Mar Res 67(4):663–674. https://doi.org/10.1007/s10152-013-0352-5